Photoresponsive Helical Foldamers: Conformational Control through Double Helix Formation and Light-Induced Protonation

Louis Hardoin, Rana Kdouh, Youssef Aidibi, Soussana Azar, Benjamin Siegler, Magali Allain, Sébastien Goeb, Eric Levillain, Pierre-Antoine Bouit, Olivier Galangau, et al.

Chemistry–A European Journal
Research Article
doi.org/10.1002/chem.202403771
Chemistry Europe
European Chemical Societies Publishing
www.chemeurj.org

Photoresponsive Helical Foldamers: Conformational Control Through Double Helix Formation and Light-Induced Protonation

Louis Hardoin,[a] Rana Kdouh,[a] Youssef Aidibi,[a] Soussana Azar,[a] Benjamin Siegler,[a] Magali Allain,[a] Sébastien Goeb,[a] Eric Levillain,[a] Pierre-Antoine Bouit,[b] Olivier Galangau,*[b] Marc Sallé,*[a] and David Canevet*[a]

Helical foldamers constitute particularly relevant targets in the field of host-guest chemistry, be that as hosts or substrates. In this context, the strategies reported so far to control the dimensions and shape of foldamers mainly involve modifications of the skeleton through covalent synthesis. Herein, we prepared an oligopyridine dicarboxamide foldamer substituted by photo-active tetraphenylethylene units (TPE). We demonstrate that it is possible to toggle the length of a helical foldamer by two means. First, the elongation of foldamers can be tuned by adjusting the concentration, as demonstrated by DOSY NMR spectroscopy and X-ray diffraction analyses on both the single and the double helix structures. Secondly, and in a more original manner, a photo-induced protonation process triggered by TPE units promotes a novel pathway to unfold helical foldamers, leading to dramatic conformational and spectroscopic changes.

Introduction

Since the early 1990s, foldamers have emerged as an important family in supramolecular chemistry.[1–3] These oligomer strands adopt various well-defined secondary structures,[4] such as sheets, turns and others. Among this wide range of possible arrangements, helical structures are the most prominent ones.[5] The folding into helices results into the formation of an inner cavity, which has allowed to bind a wide range of guests to date and sometimes, with impressive binding constants even in competing solvents, as well as outstanding selectivities.[6,7] This justifies why continuous efforts have been dedicated into controlling the shape and the conformation of these helical structures, in order to explore their potential towards various applications such as sensing,[8–12] purification processes[13,14] or catalysis,[15] for instance. In addition, controlling the conformation and assemblies made up of helical foldamers may have a strong impact in therapeutics, since some of them were shown to inhibit protein-protein interactions[16–23] and can be used as auxiliary agents to organize proteins into complex assemblies.[24,25]

Since their ability to fold into well-defined secondary structures results from noncovalent bonds, foldamers are dynamic by nature and hence, stimuli-responsive. This feature allows for controlling their properties on condition to develop efficient strategies to tune their shapes and/or conformations. As far as helical foldamers are concerned, it is also worth noting that important structural rearrangements may also occur through double helix formation, which occurs when foldamer strands associate to form multiple helices.[26–28] From the dimensions point of view, this process is indeed accompanied by an extension of the helical backbone, as well as a slight but significant decrease of the helix diameter.[29]

In this context, relevant strategies to control the structure of helical backbones have been reported by various research groups, either by stimulations of single-stranded structures or by tuning the single-to-multiple helix equilibrium. In this sense, variations of solvent composition,[30–33] concentration,[34,35] and temperature[32,36] have definitely shown their relevance. Other chemical stimulations, such as pH variations,[37–40] metal coordination,[41,42] variation of ionic strength,[43] or guest binding[43–46] also proved meaningful. Recently, our group and others have shown to which extent redox processes[47] or photostimulation may constitute interesting opportunities to control chiroptical properties,[48,49] guest binding,[45,50] and helical multiplicity[45,46,49] in a reversible manner.

On the other hand, tetraphenylethylene (TPE) constitutes a remarkable luminescent unit in various capacities: *i*) it is easily synthesized[52] and its stability is well-documented,[53,54] *ii*) it displays an aggregation-induced emission, because photochemical reactions, which are non-radiative relaxation processes, may be impeded in cumbersome environments and favored in diluted conditions, and *iii*) these features make it

[a] L. Hardoin, R. Kdouh, Dr. Y. Aidibi, Dr. S. Azar, B. Siegler, Dr. M. Allain, Dr. S. Goeb, Dr. E. Levillain, Prof. M. Sallé, Prof. D. Canevet
Univ Angers, CNRS, MOLTECH-ANJOU-UMR 6226, F-49000 Angers, France
E-mail: marc.salle@univ-angers.fr
david.canevet@univ-angers.fr

[b] Dr. P.-A. Bouit, Dr. O. Galangau
Univ Rennes, CNRS, ISCR-UMR 6226, F-35000 Rennes, France
E-mail: olivier.galangau@univ-rennes.fr

Supporting information for this article is available on the WWW under https://doi.org/10.1002/chem.202403771

particularly appealing as solid-state emitter[55] in the fields of organic light emitting diodes (OLEDs),[56] or as probe in sensing[57] and biological imaging.[58] With this in mind, we designed foldamer **A** (Scheme 1), which includes tetraphenylethylene probes at its extremities, in view to tune its luminescent properties according to its single or double helical state. The specific formation of the double *vs* the single stranded form could be achieved in solution, as characterized by DOSY NMR using an uncommon cylindrical model, as well as in the solid-state, by X-ray diffraction analyses. Though no particular modification of the luminescent properties could be evidenced upon double helix formation or dissociation, the photochemistry of TPE offered a unique opportunity to unfold the helical structure through an original photoinduced protonation process, which can be reversed under basic conditions.

Results and Discussion

The synthesis of foldamer **A** was performed according to Scheme 2. First, **TPE-CO_2H**[52] was converted into the corresponding acyl chloride in the presence of oxalyl chloride and a catalytic amount of dry dimethylformamide, and reacted with amine **1**.[48] This allowed for isolating amide **2** (64% yield), which was subsequently converted into carboxylic acid **3** with an excellent yield. Eventually, target compound **A** was obtained through an amide coupling[59] involving **3** and diamine **4** (79% yield).[47] Along this study, a reference tetraphenylethylene derivative **5** was synthesized (ESI). The structure of all intermediates and foldamer **A** were confirmed through standard characterization techniques (See ESI).

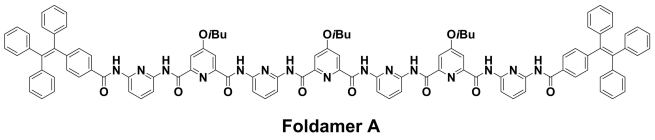

Scheme 1. Chemical structure of target foldamer **A**.

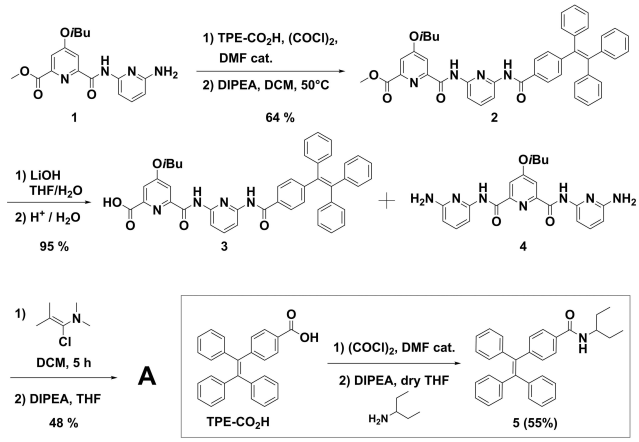

Scheme 2. Synthetic scheme leading to foldamer **A** and reference **5**.

Dissolving **A** into acetone surprisingly led after few seconds to the formation of single crystals and allowed for solving a crystallographic structure of **A** in the single helical state (Figures 1a, S1 and Movie S1). Alternatively, a slow diffusion of methanol into a chloroform solution of **A** afforded the double helical state (Figures 1b, S1 and Movie S1). Both forms crystallized as racemates in the P-1 centrosymmetric space group, which indicates that crystals contain equal amounts of *P* and *M* helices in the former case, and *P,P* and *M,M* double helices in the latter one (Table S1). Their respective X-ray crystal structures allowed to determine the helix pitch in each case. A value of 3.47 Å is observed for the single helix, characterizing a tight stacking mode within the helix loops, whereas a value of 7.34 Å (*i.e.* approximately double), is observed for the double helix (Figure S1). Those distances illustrate the high compactness degree in both objects.

Aiming at controlling the shape of foldamer **A** through double-helix formation, a first step consisted in assessing its capability to form double helices through variable-concentration ^{1}H NMR experiments. Since oligopyridine dicarboxamide foldamers commonly form double helical structures in chloroform with well-defined spectroscopic signatures, this solvent was chosen to lead the corresponding measurements at room temperature. In these conditions, single and double helices were in slow exchange at the NMR time scale (298 K, 300 MHz) (Figure 2). At high concentrations (*e.g.* 42 mM), two sets of signals were clearly observed (Figure 2 and S2). As evidenced with NH signals, a predominant set corresponding to the double helix is observed between 9.8 and 10.1 ppm,[34,48] and a minor one, associated to single helices, appeared at lower fields (above 10.2 ppm). This was further confirmed upon sample dilution down to 0.3 mM, which showed that double helices are fully dissociated at low concentrations (Figure S2). The presence of two sets of signals allowed for determining an equilibrium constant K_{dim} of 140 ± 4 for double helix formation through nonlinear curve fitting (Figures S2 and S3). In order to assess the dimensions of these molecular and supramolecular objects in solution, DOSY NMR experiments were performed (Figures 2, S3 and S4). Given the shapes and the rigid conformations of foldamer **A** and of the double helix assembly $\mathbf{A}_2$ in chloroform, we envisaged two distinct geometrical models to fit the data, *i.e.* a spherical model[60] and a cylindrical one[61] (Table S2).

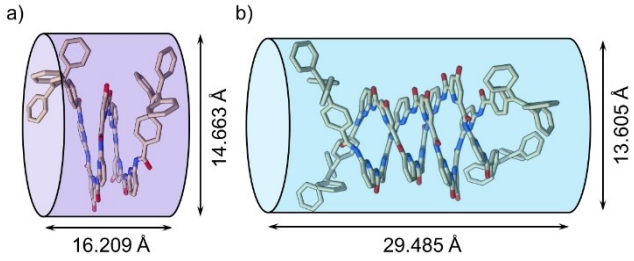

Figure 1. Crystallographic structures (Movie S1) of foldamer **A** as a single helix ((a), *M* configuration) and as a double helix ((b) *P,P* configuration) and the corresponding cylinders dimensions as extracted from DOSY NMR. Solvent molecules and isobutoxy chains are omitted for clarity.

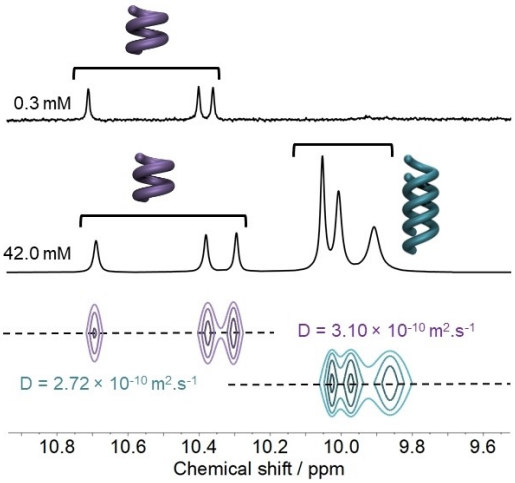

Figure 2. ^{1}H NMR spectra of foldamer **A** at 0.3 mM and 42 mM ($CDCl_3$, 298 K, 500 MHz) and the corresponding DOSY NMR spectra recorded in the same conditions (42 mM). Minor variations of chemical shifts result from intermolecular contacts.

The best fits were systematically obtained with the cylindrical model, which appears reasonable with regard to the foldamer shapes (Tables S3 and S4). An important feature of these objects lies on the change of their size upon double helix formation (*i.e.* elongation – contraction along and perpendicular to the helix axis (Figure 1)). In Figure 3 are represented the crystallographic structures of foldamer **A** in the single and double helical states, as well as cylinders whose dimensions were calculated thanks to DOSY NMR data (Table S4). In the single helical state, a diameter of 14.663(23) Å was determined from these DOSY experiments, while the double helical structure displayed a 13.605(5) Å. This corresponds to a 11% decrease of the diameter. On the other hand, the length of the foldamer structures, either determined from the X-ray structures[62] or by fitting DOSY NMR data, significantly varies, from *ca* 16.209(43) Å to 29.485(34) Å upon double helix formation. This corresponds to a 82% elongation process and confirms that this supramolecular process constitutes a relevant tool to tune the geometry of helical foldamers and hence, to control its assembling properties.

An important characteristic of the TPE unit lies on well-established luminescent properties.[55] The spectroscopic properties of foldamer **A** were studied and no particular modification of its emission spectrum could be evidenced when varying the concentration of foldamer. Nevertheless, these experiments unveiled an interesting photochemical transformation upon exposure to UV irradiation. In fact, irradiating a solution of foldamer **A** in a continuous manner (λ_{exc} = 309 nm) provoked the progressive disappearance of the 309 nm absorption band and the appearance of new absorption bands centered at 260 and 360 nm (Figure 3a). It is worth noting that an increase in the fluorescence intensity was concomitantly observed, at blue-shifted wavelength compared to the expected TPE luminescence, though the absorption at 309 nm decreased (Figure 3b).

To the best of our knowledge, such a light-promoted behavior had never been described in the oligopyridine

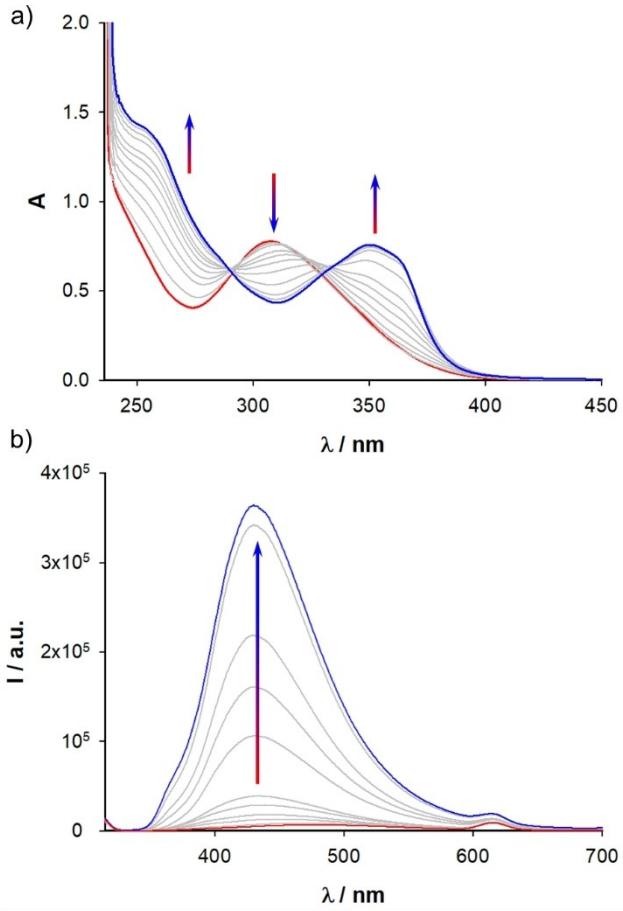

Figure 3. Evolutions of absorption (a) and emission (b) spectra of foldamer **A** under UV- irradiation (313 nm) (red line = before irradiation, blue line = after irradiation), $CHCl_3$, C = 2.5×10^{-5} mol.L^{-1}, l = 1 cm, λ_{exc} = 309 nm.

dicarboxamide series, and therefore a photochemical reaction involving TPE units was considered. This chromophore is actually known for undergoing the so-called Mallory reaction, which consists in a photoinduced cyclization reaction followed by an oxidation process leading to phenanthrene derivatives.[63,64] This prompted us to study the impact of UV irradiation (λ_{exc} = 309 nm) on a) reference **5**, which does not include any foldamer fragment, b) intermediate **2** and c) foldamer **B** (Scheme S1), which does not include any TPE unit.

As anticipated, irradiating foldamer **B** did not lead to any significant evolution of its absorption spectrum, which implies that the foldamer skeleton is not involved in the photochemical process. On the contrary, reference compound **5** (Scheme 2) exhibited an absorption band centered at 325 nm that decreased upon irradiation to the benefit of a new absorption band at 260 nm (Figure S5), and which is similar to the higher energy band observed upon irradiation of foldamer **A**. As reported in the literature for pristine tetraphenylethylene, this band constitutes a spectroscopic signature of the corresponding photocyclized species. At this stage, one will also note that such continuous irradiation also led to an increased fluorescence intensity (Figure S6), which is expected along the formation of the corresponding phenanthrene derivative.[65]

On this basis, irradiation of intermediate **2** was conducted at a semi-preparative scale and allowed for isolating the photocyclized compound $\mathbf{2}_{PC}$ (Scheme S2 and experimental details), confirming the occurrence of the Mallory reaction. In addition, the photocyclization of TPE units after irradiation of foldamer **A** was also confirmed by mass spectrometry with the observation of a peak corresponding to $[\mathbf{A}–4H+Na]^+$ (m/z = 1780.7) (Figure S7). Eventually, the UV exposure of intermediate **2** also proved valuable to get insight on the appearance of the absorption band at lower energies (Figure S8). Unlike the case of TPE **5**, a new absorption band centered at λ = 360 nm appeared when exciting solutions of intermediate **2**, thus highlighting the contribution of the foldamer skeleton in the appearance of this new electronic transition. Since TPE photocyclization remains scarcely reported in the literature with regard to the hundreds of papers reporting its luminescent properties, the quantum yields of photocyclization were determined for **2**, **5** and **A** (Table 1, Figures S8–10).[65] The Φ_{PC} appeared drastically lower in the case of the oligopyridine dicarboxamide derivatives (compound **2** and foldamer **A**), which illustrates a decreased photocyclization ability and hence, the absence of energy transfer from the foldamer skeleton to the tetraphenylethylene units.

Table 1. Quantum yields of photocyclization ($CHCl_3$, 20 °C, λ_{irr} = 313 nm).

	2	TPE **5**	Foldamer **A**
φ_{PC}^{313}	0.0009	0.025	0.0005

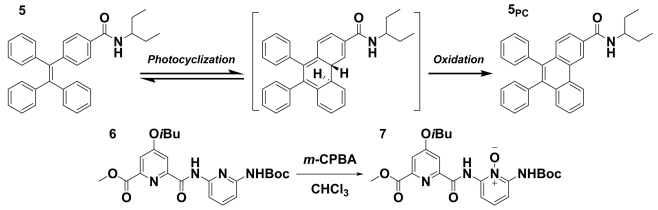

Scheme 3. a) Photocyclization-oxidation process represented in the case of **5**. b) Synthesis of *N*-oxide **7**.

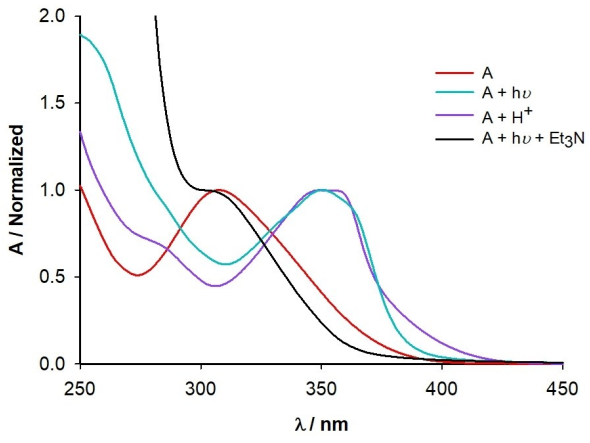

Figure 4. Normalized absorption spectra of foldamer **A** before (red curve), after irradiation (blue curve), after protonation (purple, 80 eq. of TFA) after irradiation and addition of triethylamine (black, 20 eq.) $CHCl_3$, $C = 2.5\times10^{-5}$ mol.L^{-1}, l = 1 cm, λ_{exc} = 309 nm.

To explain the appearance of a new absorption band at λ_{max} = 360 nm, we considered the possibility that Mallory reaction could be responsible for hydrogen peroxide release, subsequent *N*-oxidation of pyridyl rings and hence, modification of the absorption spectrum. This possibility could be ruled out in a straightforward manner, by preparing *N*-oxide **7** (Scheme 3),[66] which does not display any spectroscopic signature above 330 nm (Figure S11). Since protons may also be released along the photocyclization-oxidation process,[67,68] another hypothesis lied on the protonation of foldamer pyridyl rings.[38] Therefore, two complementary experiments were performed. First, an irradiated solution of foldamer **A** was treated with a base (Et_3N), which led to the disappearance of the low energy absorption band (Figure 4). Second, trifluoroacetic acid was added to a solution of foldamer **A** (Figure S12) and the corresponding modifications of the UV-visible absorption spectrum strongly resembled those observed upon irradiation (Figures 4). Finally, the photochemical process was performed in the presence of propylene oxide (Figure S13), which is commonly used to trap generated acids along Mallory reaction.[69] In these conditions, an increase of the absorbance was observed in the UV range (~250 nm) but no additional absorption band was evidenced at *ca* 350 nm. Consequently, these experiments confirm altogether that the foldamer backbone gets protonated upon UV-irradiation. In order to identify the protonated pyridyl rings, a solution of **2** was titrated with trifluoroacetic acid and the evolution of its ^{1}H NMR spectrum was recorded (Figure S14). This experiment showed that, unlike pyridyl dicarboxamide units, diaminopyridyl fragments get protonated.

When it comes to identifying the structures adopted by foldamers, circular dichroism spectroscopy constitutes an essential technique.[68] Among various possibilities, it notably allows for determining whether the adopted arrangement is chiral or not, and identifying the handedness of helical structures. Taking advantage of this technique, Huc and Coll. showed in 2003 that pH variations allows for unfolding chiral oligopyridine dicarboxamide foldamers by partial protonation with trifluoroacetic acid.[38] With this in mind, and taking advantage of the presence of TPE units in foldamer **A**, we considered the possibility to trigger indirectly its unfolding process through photochemical stimulations.

In the absence of chiral information and in diluted solutions, foldamer **A** exists as a racemic mixture of *P* and *M* single helices. This prevents the utilization of a circular dichroism (CD) spectrometer to study conformational changes. For this purpose, a large excess of (*R*)-mandelic acid, known for its ability to induce a preferential helicity for such foldamers,[70] was added to a solution of **A** in chloroform. As evidenced by CD spectroscopy, the chiral induction phenomenon proved effective (Figure 5a) with the observation of a negative Cotton effect. Interestingly, irradiation of the solution at 313 nm led to the progressive disappearance of the dichroic signal, as reported earlier upon protonation of chiral foldamers.[38]

As shown by UV-visible absorption spectroscopy (Figure 4), irradiation and addition of trifluoroacetic acid (80 eq.) both lead to the protonation of the oligopyridine dicarboxamide strand.

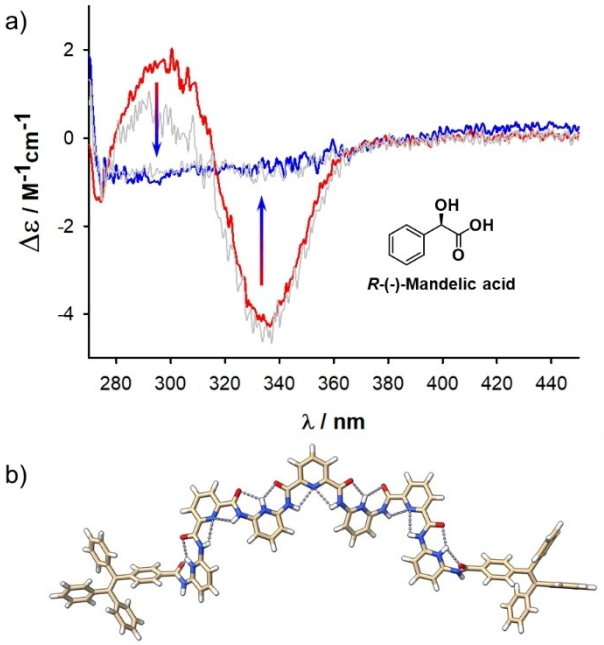

Figure 5. (a) Evolution of the CD spectra of foldamer **A** ($CHCl_3$, $C = 3\times10^{-5}$ mol.L^{-1}), $l = 1$ cm) in the presence of (*R*)-mandelic acid (200 equivalents) and upon continuous irradiation (313 nm). b) Optimized geometry of partially protonated foldamer **A** calculated through molecular mechanics (MM +). Hydrogen bonds responsible for the unfolding process in dotted lines.

Thereby, the disappearance of the CD signal may arise from the dissociation of the 'chiral guest–helical foldamer' complexes, which would result in the racemization of helical structures, or from an unfolding process. To tackle this issue, a diluted solution of **A** in the single helical state ($CDCl_3$, 0.8 mM) was treated with deuterated trifluoroacetic acid and studied by NMR spectroscopy. Before addition of acid (Figures S15–S18), NOESY experiments show through-space correlations between amide protons (Figures S17–S18), which corresponds with **A** adopting a helical conformation.[36] In this state, no correlation was observed between aromatic protons of pyridyl units and amide ones in the NOESY NMR spectrum of **A**, which appears logical with regard to the orientation of the amide protons towards the center of the helix cavity. On the other hand, the addition of trifluoroacetic acid to a solution of **A** ($CDCl_3$, 0.8 mM) revealed, 1) that, as for intermediate **2**, the diaminopyridyl fragments of **A** get protonated (Figures S19–S22), and most importantly, 2) that new correlations appear upon protonation between the protons in positions 3 and 5 of pyridinium rings and amide ones (Figures S23, S24). Consequently, these observations demonstrate, altogether, that protonation, whether it is induced chemically or photochemically, triggers a modification of the hydrogen bond network and hence, the unfolding of the foldamer backbone. The optimized geometry of the latter could be optimized through Molecular Mechanics MM^+ calculations, which evidenced the strong elongation of the foldamer strand in comparison to the initial helical conformation. Therefore, this study shows that TPE moieties act as photoacid units in these conditions, allowing for unfolding these oligopyridine dicarboxamide foldamers through light-induced protonation. To our knowledge, such a possibility had never been reported.

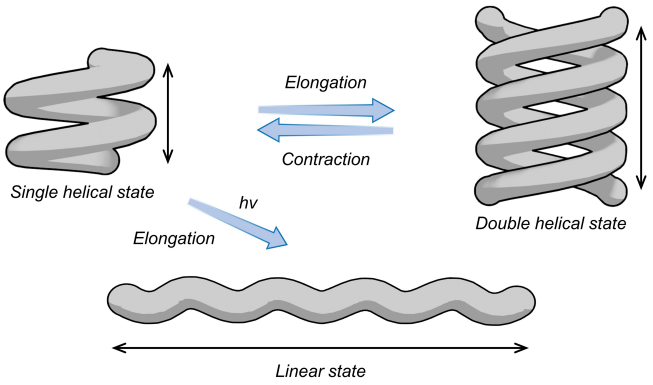

Figure 6. Shape adjustments through double helix formation or unfolding processes of an helicoidal foldamer.

Conclusions

The last decades have shown that foldamers constitute appealing structures in supramolecular chemistry, be that as hosts or substrates, as recently exemplified in combination with proteins. In this context, developing strategies to control their conformations, secondary structures and overall shape constitutes a current challenge. We herein show that the double helix formation in solution can be monitored by DOSY NMR experiments combined to relevant data processing based on a cylindrical model, as well as by single-crystal X-Ray diffraction analyses of the single and the double helical states (Figure 6). Remarkably, we show that the conformation of this TPE-based foldamer can also be controlled thanks to an original light-induced protonation mechanism (Figure 6). The latter is provoked by a simple UV irradiation process and is supported by the photoacid role of the TPE unit. We believe that this proof-of-concept could constitute an important step towards future foldamer-based receptors and to photo-responsive foldamer-based assemblies. Alternatively, optimizing the photoacidic features of TPE derivatives, based on the numerus molecular engineering strategies reported on this scaffold, could also constitute an interesting track to explore.

Acknowledgements

This work was supported by the Pays de la Loire region (ARDENT project), EUR LUMOMAT (Investissements d'Avenir ANR-18-EUR-0012) and the French National Research Agency (project n°ANR-19-CE06-0008). The authors are also thankful to the SFR MATRIX (Ingrid Freuze for mass spectrometry analyses).

Conflict of Interests

The authors declare no conflict of interest.

Data Availability Statement

The data that support the findings of this study are available from the corresponding author upon reasonable request.

Keywords: Helical foldamers · conformational control · double helix formation · photoinduced process · tetraphenylethylene

[1] S. H. Gellman, *Acc. Chem. Res.* **1998**, *31*, 173–180.
[2] S. Hecht, I. Huc, Eds., *Foldamers: Structure, Properties, and Applications*, Wiley-VCH, Weinheim, **2007**.
[3] G. Guichard, I. Huc, *Chem. Commun.* **2011**, *47*, 5933–5941.
[4] D. J. Hill, M. J. Mio, R. B. Prince, T. S. Hughes, J. S. Moore, *Chem. Rev.* **2001**, *101*, 3893–4012.
[5] E. Yashima, N. Ousaka, D. Taura, K. Shimomura, T. Ikai, K. Maeda, *Chem. Rev.* **2016**, *116*, 13752–13990.
[6] H. Juwarker, J. Suk, K.-S. Jeong, *Chem. Soc. Rev.* **2009**, *38*, 3316–3325.
[7] T. A. Sobiech, Y. Zhong, B. Gong, *Org. Biomol. Chem.* **2022**, *20*, 6962–6978.
[8] E. Arunkumar, A. Ajayaghosh, J. Daub, *J. Am. Chem. Soc.* **2005**, *127*, 3156–3164.
[9] S. Saha, B. Kauffmann, Y. Ferrand, I. Huc, *Angew. Chem. Int. Ed.* **2018**, *57*, 13542–13546.
[10] R. Hein, A. Borissov, M. D. Smith, P. D. Beer, J. J. Davis, *Chem. Commun.* **2019**, *55*, 4849–4852.
[11] Y. Zhao, Z. Zhong, *J. Am. Chem. Soc.* **2006**, *128*, 9988–9989.
[12] Z. Zhong, Y. Zhao, *Org. Lett.* **2007**, *9*, 2891–2894.
[13] L. Yuan, P. Jiang, J. Hu, H. Zeng, Y. Huo, Z. Li, H. Zeng, *Chin. Chem. Lett.* **2022**, *33*, 2026–2030.
[14] C. Dutta, P. Krishnamurthy, D. Su, S. H. Yoo, G. W. Collie, M. Pasco, J. K. Marzinek, P. J. Bond, C. Verma, A. Grélard, A. Loquet, J. Li, M. Luo, M. Barboiu, G. Guichard, R. M. Kini, P. P. Kumar, *Chem* **2023**, *9*, 2237–2254.
[15] Z. C. Girvin, S. H. Gellman, *J. Am. Chem. Soc.* **2020**, *142*, 17211–17223.
[16] E. Lenci, A. Trabocchi, *Chem. Soc. Rev.* **2020**, *49*, 3262–3277.
[17] P. Sang, J. Cai, *Chem. Soc. Rev.* **2023**, *52*, 4843–4877.
[18] V. Kleene, V. Corvaglia, E. Chacin, I. Forne, D. B. Konrad, P. Khosravani, C. Douat, C. F. Kurat, I. Huc, A. Imhof, *Nucleic Acids Res.* **2023**, *51*, 9629–9642.
[19] V. Marković, J. B. Shaik, K. Ożga, A. Ciesiołkiewicz, J. Lizandra Perez, E. Rudzińska-Szostak, Ł. Berlicki, *J. Enzyme Inhib. Med. Chem.* **2023**, *38*, 2244693.
[20] V. Corvaglia, D. Carbajo, P. Prabhakaran, K. Ziach, P. K. Mandal, V. D. Santos, C. Legeay, R. Vogel, V. Parissi, P. Pourquier, I. Huc, *Nucleic Acids Res.* **2019**, *47*, 5511–5521.
[21] L. Delaurière, Z. Dong, K. Laxmi-Reddy, F. Godde, J. Toulmé, I. Huc, *Angew. Chem. Int. Ed.* **2012**, *51*, 473–477.
[22] J. Buratto, C. Colombo, M. Stupfel, S. J. Dawson, C. Dolain, B. Langlois d'Estaintot, L. Fischer, T. Granier, M. Laguerre, B. Gallois, I. Huc, *Angew. Chem. Int. Ed.* **2014**, *53*, 883–887.
[23] J. W. Checco, S. H. Gellman, *Curr. Opin. Struct. Biol.* **2016**, *39*, 96–105.
[24] M. Vallade, M. Jewginski, L. Fischer, J. Buratto, K. Bathany, J.-M. Schmitter, M. Stupfel, F. Godde, C. D. Mackereth, I. Huc, *Bioconjugate Chem.* **2019**, *30*, 54–62.
[25] P. S. Reddy, B. Langlois d'Estaintot, T. Granier, C. D. Mackereth, L. Fischer, I. Huc, *Chem. Eur. J.* **2019**, *25*, 11042–11047.
[26] D. Haldar, C. Schmuck, *Chem. Soc. Rev.* **2009**, *38*, 363–371.
[27] V. Berl, I. Huc, R. G. Khoury, M. J. Krische, J.-M. Lehn, *Nature* **2000**, *407*, 720–723.
[28] V. Koehler, *Chem. Eur. J.* **2024**, *31*, e202402222.
[29] E. Berni, B. Kauffmann, C. Bao, J. Lefeuvre, D. M. Bassani, I. Huc, *Chem. Eur. J.* **2007**, *13*, 8463–8469.
[30] Y. Liu, F. C. Parks, W. Zhao, A. H. Flood, *J. Am. Chem. Soc.* **2018**, *140*, 15477–15486.
[31] J. Shang, Q. Gan, S. J. Dawson, F. Rosu, H. Jiang, Y. Ferrand, I. Huc, *Org. Lett.* **2014**, *16*, 4992–4995.
[32] T. Sawato, R. Yuzawa, H. Kobayashi, N. Saito, M. Yamaguchi, *RSC Adv.* **2019**, *9*, 29456–29462.
[33] B. Teng, P. K. Mandal, L. Allmendinger, C. Douat, Y. Ferrand, I. Huc, *Chem. Sci.* **2023**, *14*, 11251–11260.
[34] V. Berl, I. Huc, R. G. Khoury, J.-M. Lehn, *Chem. Eur. J.* **2001**, *7*, 2810–2820.
[35] B. Baptiste, J. Zhu, D. Haldar, B. Kauffmann, J.-M. Léger, I. Huc, *Chem. Asian J.* **2010**, *5*, 1364–1375.
[36] M. Shigeno, Y. Kushida, M. Yamaguchi, *J. Am. Chem. Soc.* **2014**, *136*, 7972–7980.
[37] E. Kolomiets, V. Berl, I. Odriozola, A.-M. Stadler, N. Kyritsakas, J.-M. Lehn, *Chem. Commun.* **2003**, *39*, 2868–2869.
[38] C. Dolain, V. Maurizot, I. Huc, *Angew. Chem. Int. Ed.* **2003**, *42*, 2738–2740.
[39] I. Okamoto, M. Nabeta, Y. Hayakawa, N. Morita, T. Takeya, H. Masu, I. Azumaya, O. Tamura, *J. Am. Chem. Soc.* **2007**, *129*, 1892–1893.
[40] W. Wang, C. Zhang, S. Qi, X. Deng, B. Yang, J. Liu, Z. Dong, *J. Org. Chem.* **2018**, *83*, 1898–1902.
[41] M. Barboiu, J.-M. Lehn, *Proc. Nat. Acad. Sci.* **2002**, *99*, 5201–5206.
[42] J. L. Algar, J. A. Findlay, D. Preston, *ACS Org. Inorg. Au* **2022**, *2*, 464–476.
[43] F. C. Parks, Y. Liu, S. Debnath, S. R. Stutsman, K. Raghavachari, A. H. Flood, *J. Am. Chem. Soc.* **2018**, *140*, 17711–17723.
[44] F. Aparicio, L. Faour, M. Allain, D. Canevet, M. Sallé, *Chem. Commun.* **2017**, *53*, 12028–12031.
[45] Y. Zhong, T. A. Sobiech, B. Kauffmann, B. Song, X. Li, Y. Ferrand, I. Huc, B. Gong, *Chem. Sci.* **2023**, *14*, 4759–4768.
[46] Q. Gan, Y. Ferrand, N. Chandramouli, B. Kauffmann, C. Aube, D. Dubreuil, I. Huc, *J. Am. Chem. Soc.* **2012**, *134*, 15656–15659.
[47] L. Faour, C. Adam, C. Gautier, S. Goeb, M. Allain, E. Levillain, D. Canevet, M. Sallé, *Chem. Commun.* **2019**, *55*, 5743–5746.
[48] Y. Aidibi, S. Azar, L. Hardoin, M. Voltz, S. Goeb, M. Allain, M. Sallé, R. Costil, D. Jacquemin, B. Feringa, D. Canevet, *Angew. Chem. Int. Ed.* **2025**, *64*, e202413629.
[49] D. Zhao, T. Van Leeuwen, J. Cheng, B. L. Feringa, *Nat. Chem.* **2017**, *9*, 250–256.
[50] C. Adam, L. Faour, V. Bonnin, T. Breton, E. Levillain, M. Sallé, C. Gautier, D. Canevet, *Chem. Commun.* **2019**, *55*, 8426–8429.
[51] A. Lutolli, M. Che, F. C. Parks, K. Raghavachari, A. H. Flood, *J. Org. Chem.* **2023**, *88*, 6791–6804.
[52] H. Zhou, Q. Ye, X. Wu, J. Song, C. M. Cho, Y. Zong, B. Z. Tang, T. S. A. Hor, E. K. L. Yeow, J. Xu, *J. Mater. Chem. C* **2015**, *3*, 11874–11880.
[53] Y. Hong, J. W. Y. Lam, B. Z. Tang, *Chem. Soc. Rev.* **2011**, *40*, 5361–5388.
[54] Y. Chen, J. W. Y. Lam, R. T. K. Kwok, B. Liu, B. Z. Tang, *Mater. Horiz.* **2019**, *6*, 428–433.
[55] I. V. Kashnik, B. Yang, S. S. Yarovoi, T. S. Sukhikh, M. Cordier, G. Taupier, K. A. Brylev, P. Bouit, Y. Molard, *Chem. Eur. J.* **2024**, *30*, e202400079.
[56] J. Huang, Y. Jiang, J. Yang, R. Tang, N. Xie, Q. Li, H. S. Kwok, B. Z. Tang, Z. Li, *J. Mater. Chem. C* **2014**, *2*, 2028–2036.
[57] D. D. La, S. V. Bhosale, L. A. Jones, S. V. Bhosale, *ACS Appl. Mater. Interfaces* **2018**, *10*, 12189–12216.
[58] R. T. K. Kwok, C. W. T. Leung, J. W. Y. Lam, B. Z. Tang, *Chem. Soc. Rev.* **2015**, *44*, 4228–4238.
[59] L. Ghosez, B. Haveaux, H. G. Viehe, *Angew. Chem. Int. Ed.* **1969**, *8*, 454–455.
[60] Y. Cohen, L. Avram, L. Frish, *Angew. Chem. Int. Ed.* **2005**, *44*, 520–554.
[61] Y. Yamauchi, Y. Hanaoka, M. Yoshizawa, M. Akita, T. Ichikawa, M. Yoshio, T. Kato, M. Fujita, *J. Am. Chem. Soc.* **2010**, *132*, 9555–9557.
[62] This distance was determined by measuring the maximum distance separating atoms parallely to the helix axis.
[63] B.-P. Jiang, D.-S. Guo, Y.-C. Liu, K.-P. Wang, Y. Liu, *ACS Nano* **2014**, *8*, 1609–1618.
[64] M. De La Hoz Tomás, M. Yamaguchi, B. Cohen, I. Hisaki, A. Douhal, *Phys. Chem. Chem. Phys.* **2023**, *25*, 18874–18888.
[65] J. Rouillon, C. Monnereau, C. Andraud, *Chem. Eur. J.* **2021**, *27*, 8003–8007.
[66] C. Dolain, C. Zhan, J.-M. Léger, L. Daniels, I. Huc, *J. Am. Chem. Soc.* **2005**, *127*, 2400–2401.
[67] A. V. Yadykov, A. G. Lvov, M. M. Krayushkin, A. V. Zakharov, V. Z. Shirinian, *J. Org. Chem.* **2021**, *86*, 10023–10031.
[68] J. B. M. Somers, A. Couture, A. Lablache-Combier, W. H. Laarhoven, *J. Am. Chem. Soc.* **1985**, *107*, 1387–1394.
[69] L. Liu, B. Yang, T. J. Katz, M. K. Poindexter, *J. Org. Chem.* **1991**, *56*, 3769–3775.
[70] V. Maurizot, C. Dolain, I. Huc, *Eur. J. Org. Chem.* **2005**, *2005*, 1293–1301.

Manuscript received: October 10, 2024
Accepted manuscript online: January 3, 2025
Version of record online: January 16, 2025